

## Stochastic Mode Representation of a Zero-Net-Mass-Flux Jet Forced Adverse Pressure Gradient Flow

V. Kitsios<sup>1,2</sup>, N. A. Buchmann<sup>1</sup>, C. Atkinson<sup>1</sup> and J. Soria<sup>1,3</sup>

<sup>1</sup>Laboratory For Turbulence Research in Aerospace and Combustion,  
Department of Mechanical and Aerospace Engineering, Monash University, Clayton 3800, AUSTRALIA.

<sup>2</sup>Centre for Australian Weather and Climate Research, CSIRO Marine and Atmospheric Research,  
107-121 Station St, Aspendale 3195, AUSTRALIA.

<sup>3</sup>Department of Aeronautical Engineering, King Abdulaziz University, Jeddah 21589, KINGDOM OF SAUDI ARABIA.

### Abstract

For the first time modes representative of the linear dynamics (Koopman) and associated nonlinear error (stochastic covariance) are calculated for a periodically forced adverse pressure gradient flow. The Koopman and stochastic covariance modes are determined from the solution of two separate eigenvalue problems, both constructed from a series of time resolved observations. The specific flow configuration is a NACA-0015 aerofoil with a periodic zero-net-mass-flux slot jet forcing at the leading edge. The aerofoil is at an angle of attack of  $18^\circ$  with a chord based Reynolds number of  $3 \times 10^4$ . Modes are calculated from high repetition rate particle image velocimetry measurements. Modes constructed from fluctuations about the time averaged baseflow are dominated by modes of temporal and spatial scale similar to that of the forcing. Modes constructed from fluctuations about the phase averaged baseflow describe interactions between the forcing and the natural variability, and oscillations in the leading edge shear layer.

### Introduction

Many engineering systems operate in the presence of adverse pressure gradients, including: aircraft wings, wind turbine blades, and any form of turbomachinery. Flow separation in any of these scenarios can lead to drastic reductions in performance and at worst catastrophic consequences. The study of separation will enable us to further understand the pertinent boundary layer physical processes, and to develop practical passive and/or active flow control devices.

The specific configuration studied within is a leading edge separated NACA 0015 aerofoil at an angle of attack of  $18^\circ$ , with a chord based Reynolds number of  $Re \equiv u_\infty c / \nu = 3 \times 10^4$ , where  $\nu$  is the kinematic viscosity,  $c$  the chord length, and  $u_\infty$  the freestream velocity. All parameters and results presented within are non-dimensionalised by  $c$  and  $u_\infty$ . The system is periodically forced by a two-dimensional zero-net-mass-flux (ZNMF) slot jet at the leading edge of frequency  $f_0 = 1.22$  and a momentum blowing coefficient of  $c_\mu = u_{j,rms}^2 h = 0.0014$ , where  $u_{j,rms}$  is the root-mean-square jet velocity and  $h$  is the jet slot width. This jet actively controls the flow, which delays separation and enhances the lift force. The experiments are conducted in a horizontal water tunnel using high repetition rate particle image velocimetry (HR-PIV) to measure the time-resolved two-component, two-dimensional velocity fields at the mid-span. In the absence of forcing, laminar flow separation occurs at the leading edge as shown in figure 1(a). In the presence of the above specified forcing a time-averaged reattachment of the flow is achieved, as illustrated in figure 1(b). A detailed description of the experiments is presented in [1, 10], and a large eddy simulation of the unforced baseflow is discussed in [6].

The focus of the present paper is to study the stability properties of the controlled aerofoil flow in the temporally periodically forced environment. Using a proper orthogonal decomposition (POD) projection method outlined within [5, 2], we construct a stochastic linear model representing the evolution of the discretely sampled (truncated) system, from the time-resolved HR-PIV measurements of [1], with a time between velocity field snapshots of  $\Delta t = 0.0067$ . We present the eigenvectors of the linear operator (Koopman modes) representing the linear dynamics, and also the eigenvectors of the covariance matrix of the stochastic force representing the fluctuations not governed by the linear operator. The general mathematical approach for computing the modes is outlined in the following section. Koopman and stochastic covariance modes are calculated for fluctuations about both the time averaged baseflow and the phase averaged baseflow. Physical interpretations made from the spatial and temporal characteristics of these modes are provided.

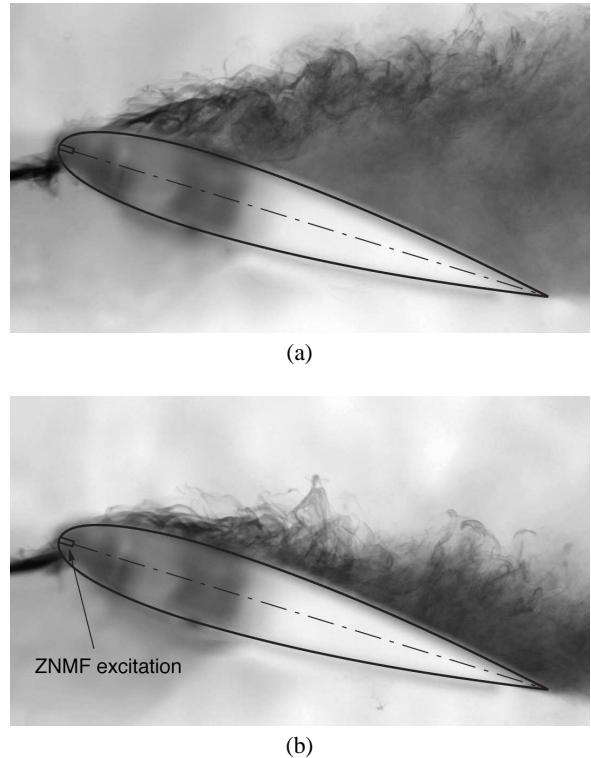


Figure 1: Dye flow visualisation [10] of a NACA-0015 aerofoil at  $\alpha = 18^\circ$  and  $Re = 3 \times 10^4$ : (a) unforced case; (b) ZNMF jet forcing at the leading edge with a forcing frequency of  $f_0 = 1.22$  and momentum blowing coefficient of  $c_\mu = 0.0014$ .

## Koopman Mode Theory

Koopman modes [7] were introduced to geophysical fluid mechanics in [4] (termed principal oscillation patterns), with a detailed review presented in [11]. Further detailed discussion on the Koopman operator in the field of engineering fluid mechanics is presented in [8, 9]. Here we follow the derivation of [3]. The approach uses observations of a general nonlinear system to construct a linear operator that best represents the evolution of the system, with the eigenvectors of the linear operator and error covariance matrix the modes of interest. However, the linear operator becomes prohibitively large for data sets with many spatial points. In the present study we alleviate this problem by projecting the eigenvalue problems onto a set of POD modes as outlined in [5]. The following discussion, however, will focus on the Koopman mode theory.

To facilitate the discussion we define the state vector  $\mathbf{u}(t)$  that contains the streamwise ( $u$ ) and vertical ( $v$ ) velocity components at all points in space at time  $t$ . It is decomposed into a potentially time varying baseflow  $\mathbf{U}^{(0)}(t)$  and the fluctuations about this baseflow  $\mathbf{u}'(t)$ . Results are presented for  $\mathbf{U}^{(0)}(t)$  equal to both the time and phase averaged baseflow.

In the Koopman mode decomposition a non-linear system is approximated by

$$\dot{\mathbf{u}}'(t) = \mathbf{M}\mathbf{u}'(t) + \mathbf{f}(t), \quad (1)$$

where  $\mathbf{M}$  is a time invariant linear operator, and  $\mathbf{f}(t)$  represents the nonlinear interactions not governed by  $\mathbf{M}$ . The estimate of  $\mathbf{M}$  that minimises the variance of  $\mathbf{f}(t)$  is given by Gauss' theorem of least squares to be

$$\mathbf{M} = \frac{1}{\Delta t} [\langle \mathbf{u}'(t + \Delta t) \mathbf{u}'^T(t) \rangle \langle \mathbf{u}'(t) \mathbf{u}'^T(t) \rangle^{-1} - \mathbf{I}], \quad (2)$$

where the angular brackets denote time averaging, and we have approximated the state time derivative as

$$\dot{\mathbf{u}}'(t) \approx \frac{\mathbf{u}'(t + \Delta t) - \mathbf{u}'(t)}{\Delta t}, \quad (3)$$

with  $\Delta t$  the time between discretely sampled snapshots. The Koopman modes are given by the solution of the eigenvalue problem

$$-i\Omega^{(j)}\mathbf{U}^{(j)} = \mathbf{M}\mathbf{U}^{(j)}, \quad (4)$$

where for each mode  $j > 0$ , the complex right eigenvector is  $\mathbf{U}^{(j)}$ , and the complex eigenvalue  $\Omega^{(j)} \equiv \Omega_r^{(j)} + i\Omega_i^{(j)}$ . The imaginary component  $\Omega_i^{(j)}$  is the growth rate, and the real component is related to the frequency  $f^{(j)}$  by  $\Omega_r^{(j)} = 2\pi f^{(j)}$ . For temporally growing modes  $\Omega_i^{(j)} > 0$ , decaying modes  $\Omega_i^{(j)} < 0$ , and marginally stable modes  $\Omega_i^{(j)} = 0$ . The left eigenvectors (adjoint modes), form a biorthogonal set with the right eigenvectors (direct modes). We use the adjoint modes to determine the contribution of each direct mode to the individual snapshots, from which we determine the amount of fluctuation energy represented by each mode ( $E^{(j)}$ ).

In addition for a system in statistical steady state with  $\langle \partial/\partial t \rangle \langle \mathbf{u}'(t) \mathbf{u}'^T(t) \rangle = 0$ , one can determine the stochastic covariance of  $\mathbf{f}(t)$ , denoted by  $\mathbf{F}$ , which is the variance of the fluctuations not governed by the deterministic linear operator  $\mathbf{M}$ . The variance  $\mathbf{F}$  is determined from (1) post-multiplied by  $\mathbf{u}'^T(t)$  added to  $\mathbf{u}'(t)$  multiplied by the transpose of (1), all time averaged, such that

$$\begin{aligned} \mathbf{F} &\equiv \langle \mathbf{f}(t) \mathbf{u}'^T(t) \rangle + \langle \mathbf{u}'(t) \mathbf{f}^T(t) \rangle \\ &= -\mathbf{M} \langle \mathbf{u}'(t) \mathbf{u}'^T(t) \rangle - \langle \mathbf{u}'(t) \mathbf{u}'^T(t) \rangle \mathbf{M}^T. \end{aligned} \quad (5)$$

One can now determine  $\mathbf{F}$  using the previously calculated  $\mathbf{M}$ . The eigensolution of the real symmetric matrix  $\mathbf{F}$  is given by

$$\sigma^{(j)} \mathbf{U}_S^{(j)} = \mathbf{F} \mathbf{U}_S^{(j)}, \quad (6)$$

where for each mode  $j > 0$ , the real eigenvalue  $\sigma^{(j)}$  represents the fluctuation energy in each mode, and  $\mathbf{U}_S^{(j)}$  is the real eigenvector capturing any spatial correlation in the error field. The modes are in order of decreasing energy. One can consider this eigenvalue problem as generating a POD of the fluctuations not governed by the linear operator  $\mathbf{M}$ .

## Modes Representative of the Linearised Dynamics

We now present the temporal and spatial properties of the linearised dynamics for fluctuations about both the time and phase averaged baseflows. The time averaged baseflow of the snapshots is calculated and subtracted away from each snapshot, from which the linear operator  $\mathbf{M}$  is calculated using (2). The phase used for the phase averaged based flow is that of the periodic forcing  $1/f_0 = 0.82$ . This time dependent baseflow is calculated and subtracted away from each snapshot, from which the linear operator  $\mathbf{M}$  is again calculated using (2).

The eigenvalues of  $\mathbf{M}$  for both baseflow cases are illustrated in figure 2(a). The cross symbols represent the time averaged case, and the filled circular symbols represent the phase averaged case. In both cases  $\Omega_i^{(j)} \leq 0$  for all  $j$ . This means that the fluctuations are either decaying or marginally stable, which one would expect for a system in a statistical steady state. For systems such as these more insight can be gained by looking at the energy ( $E^{(j)}$ ) associated with the frequency ( $f^{(j)}$ ) of each Koopman mode.

We represent the energy in each mode by a pre-multiplied ( $E^{(j)} f^{(j)}$  versus  $f^{(j)}$ ) log-linear plot in figure 2(b), as this most clearly highlights the peaks for a given frequency. For the time averaged baseflow case, the frequency of the three most energetic Koopman modes line up with the forcing frequency  $f_0$ , its first harmonic  $2f_0$ , and second harmonic  $3f_0$ , illustrated in figure 2(b) by the dashed vertical lines. The real  $v$  component of the Koopman mode with a frequency of  $f_0$  is illustrated in figure 2(c), exhibiting a train of vortex structures. The imaginary  $v$  component has structures of similar scale, but shifted downstream such that its vortex structures are out of phase with the real component. The oscillatory behaviour of the forced dynamics of frequency  $f_0$  are reconstructed by linear combinations of the real and imaginary components of this mode. The real  $v$  component of the Koopman mode with a frequency of  $2f_0$  is illustrated in figure 2(d), also exhibiting a train of vortex structures, but more densely packed and smaller in size. Likewise the imaginary  $v$  component is shifted downstream out of phase. The mode with a frequency of  $3f_0$  contains even smaller structures. In summary, the most energetic modes representing the fluctuations about the time averaged baseflow capture the external forcing applied to the system.

The phase averaged baseflow includes the dynamics with frequencies that are the same as the forcing  $f_0$  and the harmonics of the forcing. This means the fluctuations about this baseflow exclude the dominant dynamics discussed above. This is clear from figure 2(b) with the energy at frequencies  $f_0$ ,  $2f_0$  and  $3f_0$  orders of magnitude less than that observed in the previous case. The remaining modes reflect the interactions between the forcing and the natural variability. In the unforced system the frequency of the dominant natural shedding mode is  $f_n = 0.64$  [6]. Nonlinear interaction between the forcing of frequency  $f_0$ , and the natural shedding of frequency  $f_n$ , would produce fluctuations of frequencies  $f_0 - f_n = 0.58$  and  $f_0 + f_n = 1.86$ . In fact

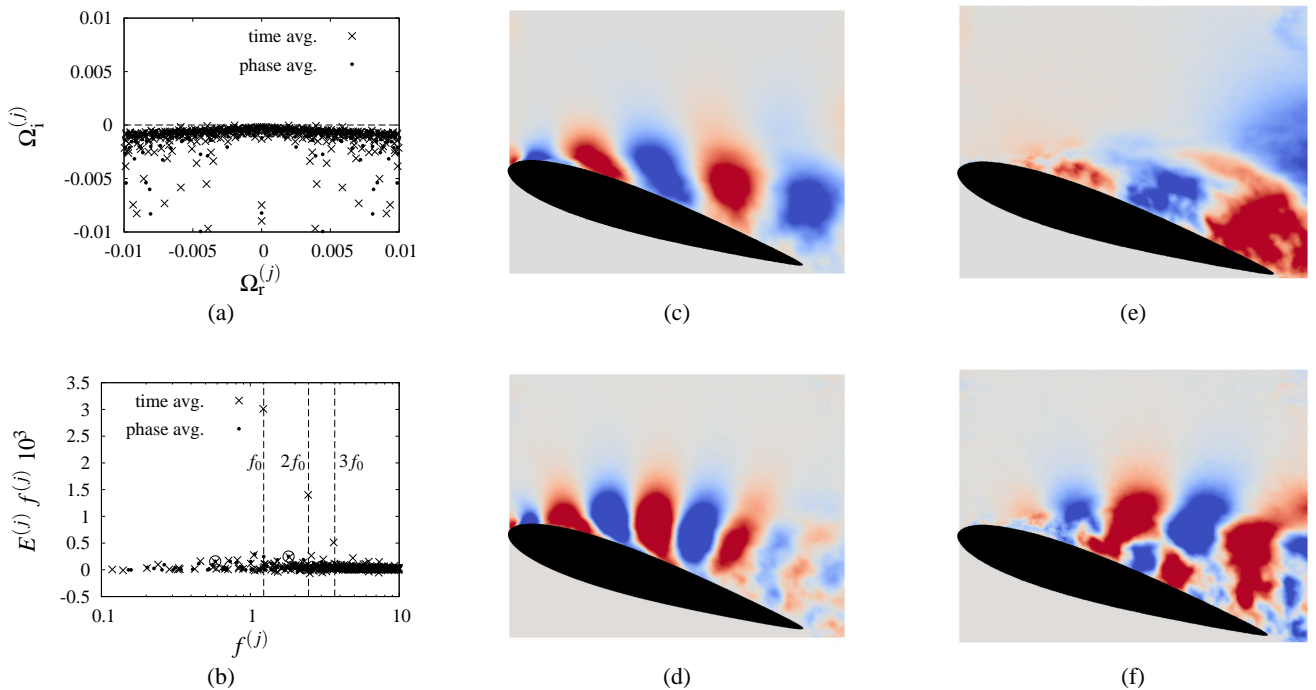


Figure 2: Deterministic dynamics about the time averaged and phase averaged baseflow. (a) Koopman eigenvalues. (b) Koopman energy versus frequency with forcing frequency  $f_0$  and harmonics  $2f_0$  and  $3f_0$  labelled. Real  $v$  component of Koopman modes with contour levels from  $-0.005$  (blue) to  $0.005$  (red) for the time averaged based flow with (c)  $f = f_0$ ; and (d)  $f = 2f_0$ ; and for the phase averaged based flow with (e)  $f = f_{ac} - f_n$ ; and (f)  $f = f_{ac} + f_n$ .

two of the most energetic modes about the phase averaged mean have these frequencies, which are both circled in figure 2(b). The real  $v$  component for the mode of frequency  $f_0 - f_n$  is illustrated in figure 2(e), which illustrates structures larger than those previously illustrated, consistent with it having a longer time scale ( $1/(f_0 - f_n)$ ). Likewise the real  $v$  component for the mode with a frequency  $f_0 + f_n$  is illustrated in figure 2(f), and has a more complex vortex structure.

From figure 2(b) it is clear from the encircled modes, that there are also coincident modes calculated about the time averaged baseflow. The respective modes also have near identical spatial forms. This indicates that the subtraction of the time averaged baseflow is sufficient to identify modes associated with the external forcing, and also those associated with the interactions between the external forcing and the dynamics of the natural unforced system. The advantage of subtracting the phase averaged baseflow will become evident after considering the stochastic covariance below.

### Modes Representative of the Stochastic Covariance

For the fluctuations about both the time and phase averaged baseflows, the eigenvalues of the stochastic covariance matrix  $\mathbf{F}$  are illustrated in figure 3(a). It is clear that the energy  $\sigma^{(j)}$  of the time averaged case is larger than that of the phase averaged case for at least the first 30 modes, after which  $\sigma^{(j)}$  of the two cases converge. This indicates that a linear stochastic model based on the fluctuations about the time averaged baseflow, has greater uncertainty than a model based on the fluctuations about the phase averaged baseflow.

This issue becomes more evident after inspecting the associated mode shapes. The most energetic mode (mode 1) for the time averaged baseflow is illustrated by the  $v$  velocity component in figure 3(b), and for the next most energetic mode (mode

2) in figure 3(c). Mode 2 has similar spatial structure and scale to mode 1 but shifted out of phase downstream. These modes have very similar spatial properties to the Koopman mode of frequency  $2f_0$  illustrated in figure 2(d). This indicates that the most significant error in the linear model of the evolution of the fluctuations, is that based on the representation of scales resembling the first harmonic. As the mode number increases, and the energy in each mode decreases, the size of the vortex structures in the associated stochastic covariance modes also decreases.

The stochastic covariance modes calculated from the fluctuations about the phase averaged baseflow have minimal resemblance to the dominant Koopman modes and the external forcing. Mode 1 is illustrated in figure 3(d), and is representative of the incoherent fluctuations distributed throughout the domain. Modes 2 contains larger yet still incoherent structures. Modes 3 through to 6 contain coherent structures representative of the small scale fluctuations centred about the leading edge shear layer, with mode 5 illustrated in figure 3(e).

Note the Koopman modes have both a coherent spatial form given by the eigenvectors  $\mathbf{U}^{(j)}$ , and a coherent temporal form given by the frequency and temporal growth rate embedded in the complex eigenvalue  $\Omega^{(j)}$ . The stochastic covariance modes, however, only have a coherent spatial form given by the eigenvectors  $\mathbf{U}_S^{(j)}$ . We know the temporal variance of each of the modes from  $\sigma^{(j)}$ , from which one could build a stochastic reduced order model of the system using the approach outlined in [12].

### Conclusions

Modes representative of the linear dynamics and stochastic covariance have been calculated from HR-PIV measurements of a NACA-0015 aerofoil flow forced at the leading edge by a ZNMF jet. Modes have been presented describing the fluctu-

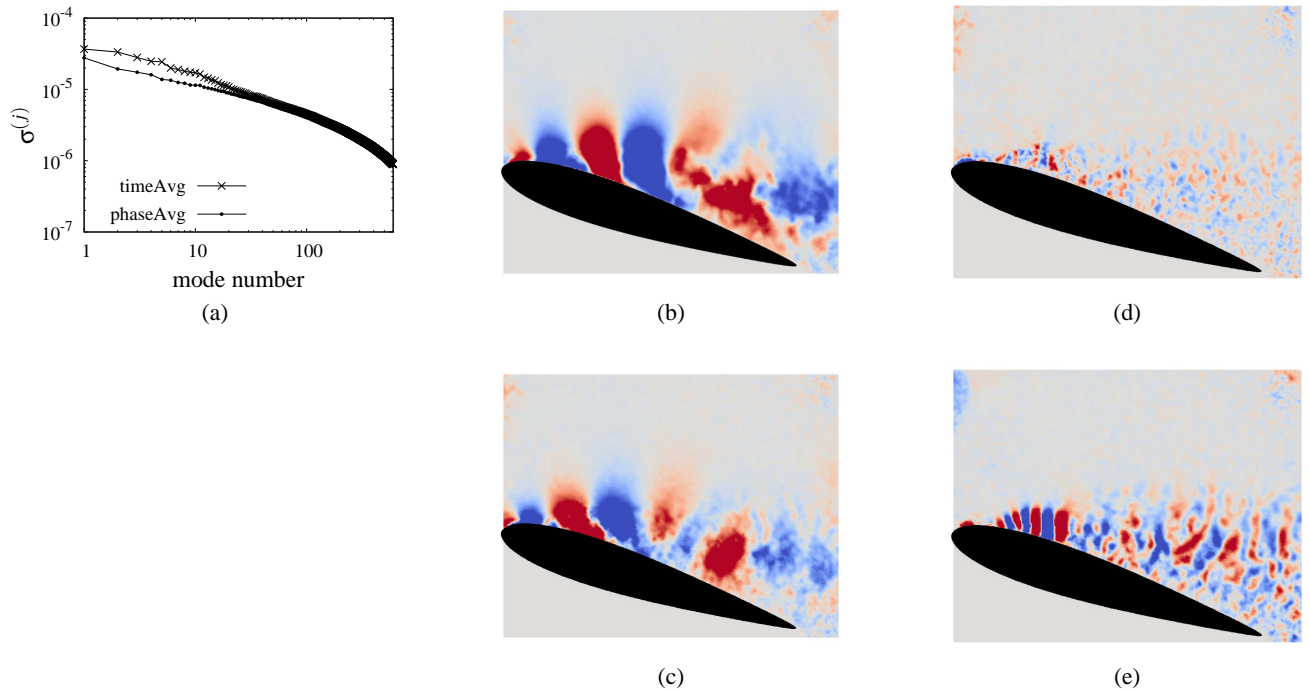


Figure 3: Stochastic dynamics about the time averaged and phase averaged baseflow. (a) Energy versus mode number. Real  $v$  component of stochastic covariance modes with contour levels from  $-0.005$  (blue) to  $0.005$  (red) for the time averaged baseflow: (b) mode 1; and (c) mode 2. For the phase averaged baseflow: (d) mode 1; and (e) mode 5;

ations about both the time and phase averaged baseflow, where the phase was taken to be that of the jet forcing. Stochastic linear models constructed from fluctuations about the time averaged baseflow are dominated by modes with temporal and spatial scale similar to that of the forcing and its harmonics. Models developed from fluctuations about the phase averaged baseflow yield dominant Koopman modes describing the interactions between the forcing and the natural variability, and dominant stochastic covariance modes representing small scale fluctuations in the leading edge shear layer.

#### Acknowledgements

The authors gratefully acknowledge the financial support of the Australian Research Council through the Discovery Project.

#### References

- [1] Buchmann, N., Atkinson, C., & Soria, J., Influence of ZNMF jet flow control on the spatio-temporal flow structures over a NACA-0015 airfoil. *Exp. Fluids*, **54**, 2013, 1485–1498.
- [2] Buchmann, N. A., Kitsios, V., Atkinson, C., & Soria, J., Investigation of coherent structures and dynamics using POD and DMD of a separated airfoil subjected to ZNMF jet forcing, in *Instability and Control of Massively Separated Flows*, editors Theofilis, V. and Soria, J., Springer International Publishing, in press.
- [3] Frederiksen, J. S. & Branstator, G., Seasonal variability of teleconnection patterns. *J. Atmos. Sci.*, **62**, 2005, 1346–1365.
- [4] Hasselmann, K., PIPs and POPs: The reduction of complex dynamical systems using principal interaction and oscillation patterns. *J. Geophys. Research*, **93**, 1988, 11015–11021.
- [5] Kitsios, V., Buchmann, N. A., Atkinson, C., Frederiksen, J. S. & Soria, J., Recovery of the Koopman Modes of a Leading-Edge Separated Aerofoil Flow via a Proper Orthogonal Decomposition Rank Reduction, in *Instability and Control of Massively Separated Flows*, editors Theofilis, V. and Soria, J., Springer International Publishing, in press.
- [6] Kitsios, V., Cordier, L., Bonnet, J.-P., Ooi, A., & Soria, J., On the coherent structures and stability properties of a leading edge separated airfoil with turbulent recirculation. *J. Fluid Mech.*, **683**, 2011, 395–416.
- [7] Koopman, B.O., Hamiltonian systems and transformations in Hilbert space. *Proc. N. A. S.*, **17**, 1931, 315–318.
- [8] Mezić, I., Spectral properties of dynamical systems, model reduction and decompositions. *Nonlinear Dynamics*, **41**, 2005, 309–325.
- [9] Rowley, C.W., Mezić, I., Bagheri, S., Schlatter, P., & Henningson, D.S., Spectral analysis of nonlinear flows. *J. Fluid Mech.*, **641**, 2009, 115–127.
- [10] Tuck, A. & Soria, J., Separation control on a NACA 0015 airfoil using a 2D micro ZNMF jet. *Air. Eng. Aero. Tech.*, **80**, 2008, 175–180.
- [11] von Storch, H., Burger, G., Schnur, R., & von Storch, J.-S., Principal oscillation patterns: a review. *J. Climate*, **8**, 1995, 377–390.
- [12] Zidikheri, M. J. and Frederiksen, J. S., Stochastic subgrid parameterizations for simulations of atmospheric baroclinic flows. *J. Atmos. Sci.*, **66**, 2009, 2844–2858.